The FASEB Journal article fj.10-174755. Published online March 30, 2011.

In vivo tissue engineering of functional skeletal muscle by freshly isolated satellite cells embedded in a photopolymerizable hydrogel

Carlo Alberto Rossi,[*,‖] Marina Flaibani,[†,¶] Bert Blaauw,[‡,¶] Michela Pozzobon,[*] Elisa Figallo,[†] Carlo Reggiani,[‡] Libero Vitiello,[§] Nicola Elvassore,[†,¶,1] and Paolo De Coppi[*,‖,1]

[*]Stem Cell Laboratory, Department of Pediatrics, [†]Department of Chemical Engineering, [‡]Department of Human Anatomy and Physiology, and [§]Department of Biology, University of Padova, Padua, Italy; [‖]Surgery Unit, Institute of Child Health, University College London, London, UK; and [¶]Venetian Institute of Molecular Medicine, Padua, Italy

ABSTRACT **The success of skeletal muscle reconstruction depends on finding the most effective, clinically suitable strategy to engineer myogenic cells and biocompatible scaffolds. Satellite cells (SCs), freshly isolated or transplanted within their niche, are presently considered the best source for muscle regeneration. Here, we designed and developed the delivery of either SCs or muscle progenitor cells (MPCs) *via* an *in situ* photo-cross-linkable hyaluronan-based hydrogel, hyaluronic acid–photoinitiator (HA-PI) complex. Partially ablated tibialis anterior (TA) of C57BL/6J mice engrafted with freshly isolated satellite cells embedded in hydrogel showed a major improvement in muscle structure and number of new myofibers, compared to muscles receiving hydrogel + MPCs or hydrogel alone. Notably, SCs embedded in HA-PI also promoted functional recovery, as assessed by contractile force measurements. Tissue reconstruction was associated with the formation of both neural and vascular networks and the reconstitution of a functional SC niche. This innovative approach could overcome previous limitations in skeletal muscle tissue engineering.—Rossi, C. A., Flaibani, M., Blaauw, B., Pozzobon, M., Figallo, E., Reggiani, C., Vitiello, L., Elvassore, N., De Coppi, P. *In vivo* tissue engineering of functional skeletal muscle by freshly isolated satellite cells embedded in a photopolymerizable hydrogel. *FASEB J.* 25, 000–000 (2011). www.fasebj.org**

Key Words: muscle ablation · muscle reconstruction · biocompatible scaffold · cell transplantation

Reconstruction of skeletal muscle after injury or in pathological conditions remains a complex and unsolved task, despite the present knowledge of the biological processes underlying muscle regeneration (1). *In vitro* approaches based on fabrication of functional muscle before *in vivo* transplantation showed several limitations (2), due to the intrinsic complexity of large-organ reconstruction. Besides, it is well established that in mammals, skeletal muscle can repair its damaged areas only in the presence of a supporting scaffold (3).

In this perspective, the aim of our work was to combine myogenic cells and biocompatible scaffolds for developing an efficient *in vivo* strategy to restore mass loss in partially ablated muscle. In particular, we focused on a simple, robust, and reproducible technique that could be easily adapted to clinical requirements.

In response to muscle damage, the canonical myogenic precursors [satellite cells (SCs); see ref. 4] begin to proliferate and originate large numbers of muscle progenitor cells (MPCs), which contribute to fiber repair and *de novo* formation (5). At the same time, SCs replenish the compartment of quiescent cells, likely through a self-renewal mechanism (6).

MPCs can be easily isolated and expanded in culture, where they can fuse and generate myotubes (1). However, when muscle regeneration has been attempted by direct MPC injection, results have been quite disappointing; MPCs rapidly lost their myogenic potential on *in vitro* expansion and displayed high mortality on *in vivo* delivery (7). On the contrary, freshly isolated SCs, obtained using various methodologies, showed to better maintain their myogenic potential (8, 9). In particular, delivering SCs through their parental myofibers or immediately after harvesting massively improved regeneration and niche reconstitution in diseased or damaged muscles (9).

So far, these strategies have not been adopted for muscle reconstruction after ablation. In this case, a

[1] Correspondence: P.D.C., Surgery Unit, UCL Institute of Child Health, 30 Guilford St., London WC1N 1EH, UK. E-mail: p.decoppi@ich.ucl.ac.uk; N.E., Chemical Engineering Department, University of Padova, via Marzolo 9, 35131, Padova, Italy. E-mail: nicola.elvassore@unipd.it

doi: 10.1096/fj.10-174755

This article includes supplemental data. Please visit *http://www.fasebj.org* to obtain this information.

tissue engineering approach would require the delivery of cells in a 3-dimensional (3D) environment able to support *in vivo* their myogenic potential. Natural and synthetic polymeric 3D scaffolds have been tested for cell delivery in skeletal muscle, but they showed limited diffusion, fibrosis, low cellular survival and their implantation required open surgery (10–12). More recently, injection of cell-loaded biomaterials capable of being delivered through minimally invasive techniques has been envisaged (13).

Here, we explored the use of a novel type of cell scaffold, namely a photopolymerizable hydrogel based on hyaluronic acid, to deliver various types of myogenic progenitors in partially ablated murine muscles.

MATERIALS AND METHODS

Animals

Four-month-old wild-type mice [strain C57BL/6J; Jackson Laboratories, Bar Harbor, ME, USA] mice and 2-mo-old GFP transgenic mice [strain C57BL/6-Tg(ACTB-EGFP)1Osb/J; Jackson Laboratories] were used. Animals were housed and surgically treated at the Animal Colony of the Centro Interdipartimentale Vallisneri, University of Padova, under the conditions specified by the relevant Italian bylaws.

Hydrogel preparation and characterization

The hyaluronic acid–photoinitiator (HA-PI) complex is a hyaluronan ester obtained by chemical reaction between hyaluronic acid and 1-[4-(2-hydroxyethoxy)-phenyl]-2-hydroxy-2-methyl-1-propane-1-one (HHMP; Irgacure 2959), which behaves as photoinitiator during the hydrogel cross-linking. HA-PI was synthesized by Fidia Advanced Biopolymers S.p.a (Abano Terme, Italy). Solution of HA-PI in physiological solution at the specified concentrations was prepared and sterilized in autoclave. A Bluewave50 lamp (Dymax, Torrington, CT, USA) provided with a water probe (0.5 cm diameter) emitting a 366-nm conical beam was used for hydrogel cross-linking.

Rheological analysis

A rheometer (Rheostress RS150; Haake, Düsseldorf, Germany) was used to evaluate viscoelastic and rheological properties. It was equipped with a temperature control (20.0±0.5°C) and a plate-cone sensor (1°) of 60 mm diameter. During measurements, the distance between cone and plate was ~0.05 mm. The rheological behavior of the solution (before irradiation) was evaluated by analyzing the shear stress as function of rising deformation rates (0–5 s^{-1}). From measurements on cross-linked hydrogels, elastic (G') and viscous (G'') modules were calculated as function of rising oscillation frequencies (0.1–10 Hz) at constant shear stress (τ=1 Pa). Samples of different concentrations (10, 20, and 30 mg/ml) and exposition times (3 s to to 5 min) were analyzed.

Maximum flow rate

The data of viscosity μ of HA-PI solutions were used to evaluate the maximum injection flow rate Q_{max} as follows:

$$Q_{max} = \frac{\pi R^3 \tau_{max}}{4\mu}$$

where R is the needle radius that is correlated with the needle gauge, and τ_{max} is the higher shear stress allowed (1 Pa, see ref. 14).

Mesh size evaluation

Following the Flory-Rehner calculations, experimental data of hydrogel swelling can be used to calculate some important structural parameters of the hydrogel, such as the mesh size ξ (nm), defined as the length of the polymer chain between two following cross-links.

Swelling experimental data were obtained using disks of hydrogel of 22 mm diameter that were gently dried at 37°C, weighed, and then rewetted with 10 ml of physiological solution. The disks were weighed 3 d after dipping, when the equilibrium conditions were reached.

The hydrogel mesh size was calculated with the following equation (15):

$$\zeta = Q_v^{1/3} \sqrt{r_0^2}$$

where Q_v is the volumetric swelling ratio obtained from experimental data, and $\sqrt{r_0^2}$ is the root mean square distance between cross-links (nm). For HA, the following value was reported (15):

$$\zeta = 0.1707 \sqrt{M_c} Q_v^{1/3}$$

The average molecular weight M_c was calculated using a simplification of Flory-Rehner equation (16):

$$Q_v^{5/3} = \frac{\upsilon M_c}{V_1} (0.5 - \chi)$$

where υ is the specific volume of dry polymer (0.893 cm^3/g), V_1 is the specific volume of solvent (1 cm^3/g), and χ is the Flory interaction parameter between polymer and solvent (0.473).

Hydrogel morphology

The morphology of cross-linked structure was analyzed by scanning electron microscopy (JSM-6490; Jeol, Akishima, Japan). Solutions (2 ml) ranging from 10 to 75 mg/ml were cross-linked in multiwell Iwaki plates (Asahi Techno Glass Corp., Tokyo, Japan) of 22 mm diameter at 2 cm from the Triwood lamp (Helios Italquartz, Milan, Italy) for 5 min (4 mW/cm^2). The samples were freeze-dried, gold-sputtered, and analyzed (Lyovac GT2; Leybold-Heraeus, Old Greenwich, CT, USA).

Single-fiber isolation technique

Briefly, muscles were digested for 1 h at 37°C in 0.2% (w/v) type I-collagenase (Sigma-Aldrich, St. Louis, MO, USA), reconstituted in DMEM (high-glucose, with L-glutamine, supplemented with 1% penicillin-streptomycin, Gibco-Invitrogen, Milan, Italy). Following digestion, muscles were transferred in DMEM (low-glucose; Gibco-Invitrogen) on a horse serum (HS; Gibco-Invitrogen)-coated 10-cm dish (Falcon; BD Biosciences, San Jose, CA, USA) and gently triturated with a wide-bore pipette to release single myofibers. These were then transferred one by one in another HS-coated 10-cm dish, under a phase-contrast inverted microscope. This passage was repeated 3 times, in order to avoid contamination of interstitial, endothelial, and hematopoietic cells.

Myogenic precursor isolation

Single muscle fibers were isolated from flexor digitorum brevis (FDB), extensor digitorum longus (EDL), and soleus muscles from 2-mo-old male GFP$^+$ mice, as described previously (1). Groups of 20 myofibers were then placed in 2-ml Eppendorf tubes (Eppendorf, Hamburg, Germany) in 200 μl DMEM (low-glucose; Gibco-Invitrogen). Isolated fibers were left to sediment on the bottom for 15 min, and DMEM was removed and replaced with 15 μl of HA-PI before injection. Freshly isolated SCs were stripped off the fibers by repeated passage through a 18-gauge needle (17). SCs were centrifuged at 300 *g* with a microcentrifuge and resuspended in 15 μl of HA-PI. For myogenic precursor preparations, 20 single fibers were seeded onto a Matrigel-coated 35-mm-dish using a single-fiber culture technique (11). After SCs left their parental myofibers and started to proliferate, they were trypsinized and expanded. At P1, 1.5×10^5 cells were pelleted in 2-ml Eppendorf tubes and resuspended in 15 μl of HA-PI. Upon mixing with hydrogel, samples were kept in ice until implantation.

Surgical procedure

Four-month-old male C57BL/6J mice were anesthetized using Forane (Merial, Milan, Italy), and an ~4-mg wedge of tissue was removed by longitudinal cutting from the core of TA muscles. Removed tissue was weighed using a microbalance (Sartorius AG, Göttingen, Germany) in order to assess the repeatability of the ablation. Suspensions of cultured SCs, single fibers, and freshly isolated SCs in HA-PI were placed in the created pocket with a micropipette and then photopolymerized for 55 s with the monochromator light. After polymerization, muscle was sutured with 7/0 Vycril (Ethicon, Inc., Somerville, NJ, USA), enclosing the hydrogel within its core; skin was closed using 6/0 Prolene sutures (Ethicon). Two types of controls have been used: sham-operated (muscle with only surgical procedure) and nonoperated.

Histological and immunofluorescence analyses

Treated muscles were fixed in PFA 2% and incubated in sucrose solution. They were then frozen in 2-methyl-butane cooled in liquid nitrogen, and 10-μm-thick sections were prepared onto Superfrost slides (Thermo Scientific, Rockville, MD, USA) for hematoxylin and eosin (H&E), Masson's trichrome (Bio Optika, Milan, Italy), and immunofluorescence analyses. Slides were fixed with 4% paraformaldehyde in PBS and permeabilized with 0.5% Triton X-100 in PBS. For GFP analysis, they were directly mounted with fluorescent mounting medium (Dako, Glostrup, Denmark) containing DAPI as nuclear counterstain. For immunological analyses, mouse anti-paired box 7 (Pax7) antibody (dilution 1:50; Developmental Studies Hybridoma Bank, Iowa City, IA, USA), rabbit antil-aminin (Sigma; 1:150), mouse antifetal myosin BF-G6 (a kind gift from Prof. Stefano Schiaffino, Venetian Institute of Molecular Medicine; dilution 1:100), rabbit anti-GFP 594 (Invitrogen; 1:150), and rabbit anti-von Willebrand factor (Dako Cytomation; 1:100) were used. Where indicated, slides were also incubated with Alexa antiá-bungarotoxin 488 (Invitrogen), in order to mark the neuromuscular junctions.

Weight recovery assessment

To assess weight recovery, removed muscle tissue was weighed at the time of operation, and total muscle weight was inferred through a regression curve (see Supplemental Fig. S1). Six weeks after the operation, muscles were harvested and weighed. Relative muscle recovery was calculated using the formula $W_{6wk}/(W_o - W_r)$, where W_{6wk} is weight of muscle after 6 wk, W_o is inferred weight at operation, and W_r is removed muscle tissue weight.

Morphometric analyses

Average cross-sectional area of muscle sections was measured using Scion Image software (http://www.scioncorp.com). Centrally nucleated myofibers, GFP$^+$ myofibers, and vessels (stained positively for von Willebrand factor) were counted in muscle sections with Photoshop (Adobe Systems, San Jose, CA, USA).

Force measurement

Contractile performance of treated and control muscles was measured *in vivo* using a 305B muscle lever system (Aurora Scientific, Aurora, ON, Canada) in animals anesthetized with a mixture of tiletamine, zolazepam, and xilazine (18). Mice were placed on a thermostatically controlled table, with knee kept stationary and foot firmly fixed to a footplate, which, in turn, was connected to the shaft of the motor. Contraction was elicited by electrical stimulation of the peroneal nerve. Teflon-covered stainless-steel electrodes were implanted near the branch of the peroneal nerve as it emerges distally from the popliteal fossa. The two thin electrodes were sewn on both sides of the nerve, and the skin above was sutured. The electrodes were connected to an AMP Master-8 stimulator (AMP Instruments, Jerusalem, Israel). Isometric contractions induced by single stimuli (twitches) and by trains of stimuli (frequency 150 Hz, duration 0.5 s) were recorded.

Cell proliferation assay

Six weeks after operation, TA muscles were damaged by injecting 50 μl of 0.5% bupivacaine in water. At 3 d after injection, EdU (5-ethynyl-2′-deoxyuridine) was injected intraperitoneally (150 μl, 1 μg/μl concentration in phosphate buffer solution), according to Salic *et al.* (19). After an additional 48 h, mice were sacrificed; TA muscles were harvested and then frozen and sectioned at 10 μm. Click-iT staining (Invitrogen) for EdU-labeled cells was then carried out according to the manufacturer's instructions.

Microscope and imaging system

Phase-contrast and histological analyses were carried out using an inverted microscope (Olympus IX71; Olympus, Tokyo, Japan). Immunofluorescence analyses were performed using a direct microscope (Leica B5000; Leica Microsystems, Wetzlar, Germany).

Statistical analysis

Values are reported as means ± SE. Coupled data sets were compared by Student's *t* test. Statistical significance was accepted at values of $P < 0.05$.

RESULTS

Characterization of HA-PI

In this work, we developed a biodegradable, injectable, and photo-cross-linkable hydrogel, HA-PI, based on

ester of hyaluronic acid (a main component of the extracellular matrix, ligand of protein CD44, expressed by SCs; see ref. 11) linked to a synthetic photoinitiator (20); the latter allows the transition from liquid to gel when exposed to monochromatic UVA light at 366 nm (**Fig. 1*A***). To maximize cell survival and myogenic potential, various parameters needed to be considered. The shear stress acting on cells during injection depends on the viscosity of the solution, needle gauge, and flow rate; apparent viscosity of HA-PI solution at different concentrations was hence measured (Fig. 1*B*). The maximum injection flow rate was evaluated (see Materials and Methods) as a function of the needle gauge in order to maintain the shear stress <1 Pa, to avoid cell membrane damage (Fig. 1*C*). After light exposure, HA-PI constitutes a semisolid hydrogel (Fig. 1*D*, left panel), whose microstructure, at different concentrations, was characterized through scanning electron microscopy (Fig. 1*D*). HA-PI has the advantage of not requiring mixing between two separate solutions, as the photoinitiator and the hyaluronic acid chain is linked by one molecule. This property ensures structural uniformity at every concentration, as shown in Fig. 1*D*. Elastic modulus and dimension of the cross-linking reticulum of polymerized HA-PI (see Materials and Methods) were both dependent on the irradiated light energy up to 20 J/cm^2, whereas higher energy did not affect hydrogel properties. This finding ensured repeatability of results and defined the "safe" operative zone (Fig. 1*E*). It is important to note that the dimension of cross-linking reticulum (Fig. 1*F*) ensures free diffusion of biomolecules, thereby allowing cell-tissue crosstalk, while preventing the host's inflammatory cells from reaching the implanted cells. On the basis of *in vitro* results, we used a HA-PI concentration of 50 mg/ml and an exposure time of 55 s, with the light source at a distance of ~3 cm.

In the initial experiments, we evaluated HA-PI *in vivo* degradation rate, a crucial parameter for cell homing after delivery (21). On surgical ablation of ~15% w/w of TA muscle and polymer implantation, animals were sacrificed every 48 h in the first 8 d. Using morphometric software (see Materials and Methods), we measured the area of polymer present in H&E-stained muscle sections (**Fig. 2**). After the first 48 h, 70 ± 14% of muscle sections were filled by HA-PI, whereas after 8 d, hydrogel (14±9%) was mostly replaced by regenerating muscle formed by resident SCs and/or by connective tissue.

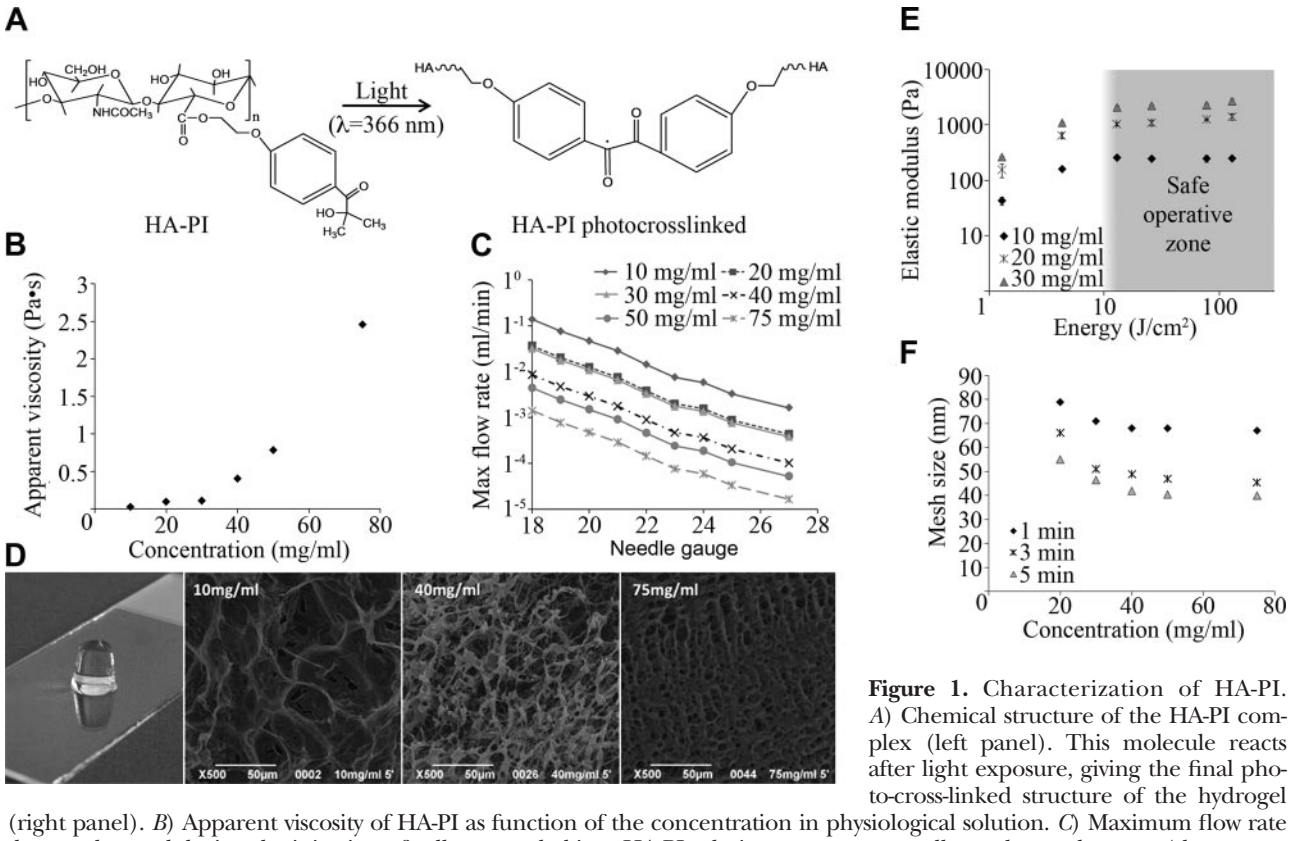

Figure 1. Characterization of HA-PI. *A*) Chemical structure of the HA-PI complex (left panel). This molecule reacts after light exposure, giving the final photo-cross-linked structure of the hydrogel (right panel). *B*) Apparent viscosity of HA-PI as function of the concentration in physiological solution. *C*) Maximum flow rate that can be used during the injection of cells suspended into HA-PI solution to ensure no cell membrane damages (shear stress ≤1 Pa). Maximum flow rate as a function of the needle gauge is reported for different HA-PI concentrations in solution. *D*) Left to right: image of a cylinder of photo-cross-linked hydrogel and scanning electron microscopy images of dehydrated hydrogel obtained from HA-PI solutions at concentrations of 10 mg/ml, 40 mg/ml, and 75 mg/ml, respectively. Scale bars = 50 μm. *E*) Elastic modulus of photo-cross-linked hydrogel as a function of the light energy used for photo-cross-linking. Values for 3 compositions of the initial solution are reported. Shaded area indicates the region where the elastic modulus does not depend on exposure energy and thus where it is "safe" to operate. *F*) Average dimensions of the cross-linking reticulum of the hydrogel as a function of HA-PI concentration. Values for 3 exposure times are reported.

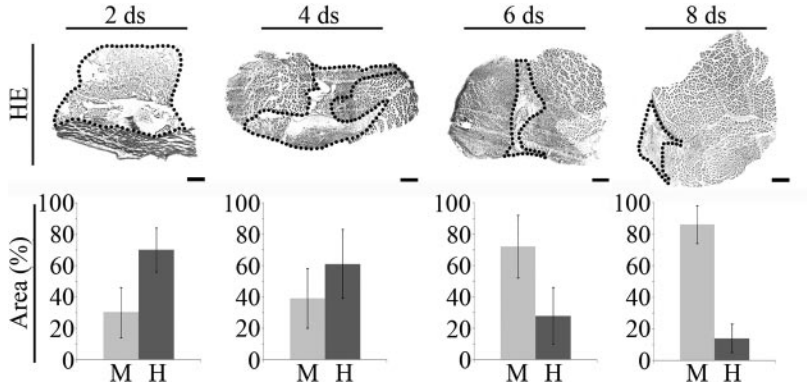

Figure 2. *In vivo* degradation study of HA-PI implanted in mouse TA muscle. Top panels: H&E staining on muscle sections 2, 4, 6, and 8 d after transplant (n=4). Scale bars = 100 μm. Bottom panels: proportion of total cross-sectional muscle area (%) occupied by muscle (M) or HA-PI (H) at the same time points.

Histological reconstruction of partially ablated TA muscle

In the *in vivo* set of experiments, 3 types of cells were delivered *via* HA-PI in partially ablated muscles: 1.5×10^5 cultured MPCs (passage 1 from a culture of 20 single fibers; see Materials and Methods and ref. 1), 20 isolated single fibers (Supplemental Fig. S2 and ref. 9) or 250 freshly isolated SCs (mechanically dissociated from 20 single fibers; see ref. 17), all derived from syngeneic C57BL/6J-GFP$^+$ mice muscles (FDB, EDL, and soleus). Fifteen days after surgery, implanted muscles were analyzed to assess muscle regeneration *vs.* infiltration (the respective areas were measured by morphometry, see Materials and Methods). Infiltration was reduced when HA-PI containing cells was used, particularly with single fibers and freshly isolated SCs (**Fig. 3*A***). Percentage of centrally nucleated fibers per section (see Materials and Methods) was also higher when fibers (97±2%) or SCs (84±8%) were used (P<0.001). MPCs (48±7%) also yielded more regenerating fibers than HA-PI alone (18±6%, P<0.001; Fig. 3*A*, right panel). Histological and morphometric analyses of muscles treated with 20 single fibers or 250 freshly isolated SCs showed extensive and consistent regeneration of the ablated region in TA muscles with little scar tissue formation after 6 wk, as evidenced by Masson's trichrome staining (Fig. 3*B*). On the contrary, sham-operated (*i.e.*, muscle ablation alone) and hydrogel-implanted muscles showed a dramatically altered morphology, with large infiltrations of connective tissue (Fig. 3*B*); muscles that received MPCs showed limited regeneration (see below). To better quantify muscle mass reconstruction, the ratio between the postoperatory weight and the preoperatory weight was also calculated (Fig. 3*B*, bottom left panel). Muscle weight at time of surgery was inferred from a regression curve plotting the correlation between TA and total body weight (n=15, Supplemental Fig. S1). Muscles treated with MPCs or SCs were heavier than sham-operated muscles (120±22 and 112±23 *vs.* 82±32%

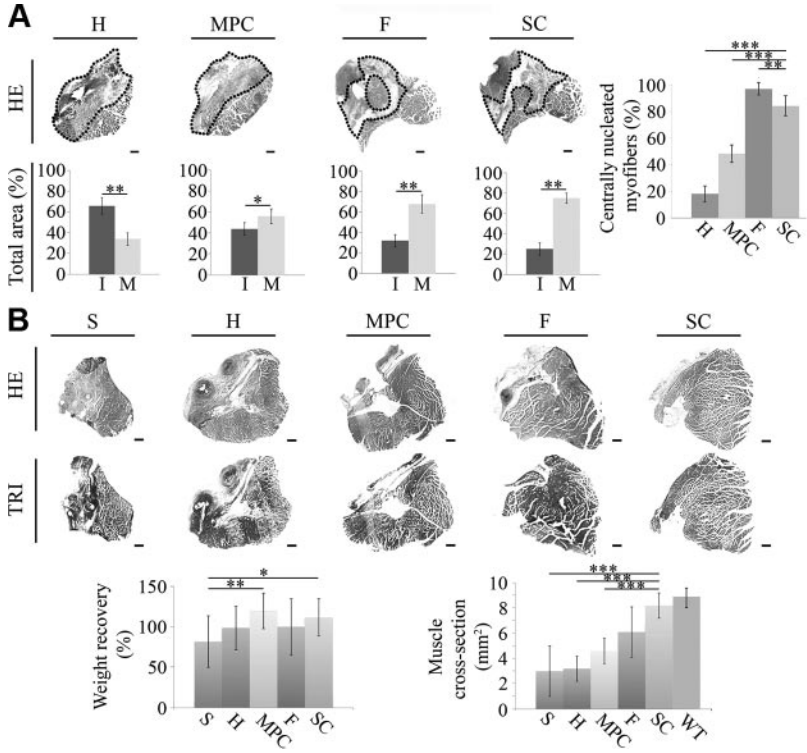

Figure 3. Histological reconstruction of partially ablated TA muscle. *A*) Histological and morphometric analysis of muscles at 15 d after treatment with HA-PI alone (H), or HA-PI with 1.5×10^5 cultured MPCs, 20 single fibers (F), or 250 freshly SCs; in all cases, 8 muscles/condition, 5 sections/muscle were analyzed. Top panels: H&E staining on muscle sections. Bottom panels: proportion of total cross-sectional muscle area (%) occupied by infiltrate (I) or muscle (M). Right panel: quantification of new myofibers in the engineered muscle (only statistics for SC are reported) showed that a higher number of centrally nucleated fibers was present when fibers (F) and SCs were used. *B*) Histological and morphometric analysis at 6 wk posttreatment. Top panels: H&E and Masson's trichrome (TRI) staining on muscle sections confirmed extensive regeneration and little scar tissue when fibers and SCs were delivered with HA-PI. F and SC, n = 10; HA-PI alone (H), n = 19; sham-operated controls (S), n = 12. Bottom left panel: weight recovery analysis (%) on treated muscles demonstrated that MPC- and SC-treated muscles were heavier than sham-operated muscles. Bottom right panel: average cross-sectional muscle area (mm^2) of treated muscles showed that only SC-treated muscles did not differ from untreated wild type. Scale bars = 100 μm. *P < 0.05; **P < 0.01; ***P < 0.001.

of recovery; $P<0.01$ and $P<0.05$, respectively), whereas HA-PI implanted (99±27%) and fiber-treated (100±35%) muscles did not show any significant difference from controls.

The average cross-sectional area of the treated muscles was also examined, in sections taken from the belly of the muscles (*i.e.*, at ~3 mm from tendons). Muscles treated with freshly isolated SCs presented a cross-sectional area of 8.2 ± 0.8 mm^2, which was bigger than sham-operated (3±1.6 mm^2; $P<0.001$), hydrogel-implanted (3.2±1.2 mm^2; $P<0.001$) and MPC-treated muscles (4.6±1 mm^2; $P<0.01$), but comparable to fiber-implanted muscles (6.1±1.5 mm^2) and non-treated wild-type animals (9.1±0.6 mm^2; Fig. 3*B*, bottom right panel). To quantify the contribution to muscle reconstruction, GFP epifluorescence was examined at 7 and 15 d and at 6 wk (**Fig. 4**); positive fibers were counted by 2 investigators in a masked procedure. Both fibers and SCs were much more effective than MPCs in contributing to neofiber formation at each time point ($P<0.001$; Fig. 4, right panel). Besides, freshly isolated SCs resulted to be more effective than single fibers both at 15 d (76±23 *vs.* 48±21, $P<0.05$) and at 6 wk (198±24 *vs.* 137±15, $P<0.001$).

Functional reconstruction of implanted muscles

We also investigated whether the implanted myogenic precursors could self-renew *in vivo* and contribute to the replenishment of the SC niche (9). *Pax7* transcription factor was used to identify SCs (**Fig. 5*A***, top panels), and laminin staining was performed to verify the sublaminal position of GFP^+ cells (Fig. 5*A*, middle panels). Percentage of $Pax7^+GFP^+$/total $Pax7^+$ cells/section ranged from 38.7 ± 4.8% in muscles reconstructed with SCs to 19.3 ± 3.8% in those receiving single fibers and just 12.6 ± 5% in those with MPCs (Fig. 5*A*). Freshly isolated SCs were, hence, the most efficient in repopulating the satellite niche ($P<0.001$). Moreover, GFP^+ SCs could be isolated from the engineered muscle *via* collagenase digestion and single-fiber culture (Fig. 5*A*, bottom panels; see Materials and Methods). To assess the distribution of engrafted SCs from the area of implant (*i.e.*, the polymer), the percentages of $Pax7^+/GFP^+$ cells associated to GFP^+ and GFP^- myofibers, respectively, were determined. We found that the percentage of GFP^+ SCs associated with GFP^- fibers was 27.3 ± 5.6% of the total in the treatment with freshly isolated SCs and 23.4 ± 4.2% in the implants with single fibers. Both values were significantly higher than the contribution given by muscle precursor cells, which stopped at 2.1 ± 0.3% (Supplemental Fig. S3). This is the first demonstration of complete functional integration in a tissue-engineered muscle, similar to what has been shown previously after cell transplantation (9). As expected, GFP^+ SCs could also be seen in *in vitro* cultures of single fibers, in which they were able to align and fuse into myotubes (Fig. 5*A*, bottom panels). Last but not least, *in vivo* activation and proliferation of GFP^+ SCs could be detected upon reinjury of treated muscles; eight 6-wk transplanted muscles were injected with bupivacaine; 5 d after damage, proliferating cells were labeled via a systemic injection of EdU (Supplemental Fig. S4).

In the last part of our study, we assessed whether macro- and microscopic histology findings were associated with functional recovery. *In vivo* force measurements were, hence, performed in animals 6 wk after treatment, with or without transplantation, and in age- and weight-matched control mice. When absolute tetanic force (150 Hz) was evaluated, there was a significant difference between treatments, with freshly isolated SCs yielding the best functional recovery (Fig. 5*B*, left). After normalization for muscle weight, the force produced by muscles treated with SCs was significantly higher when compared to other treatments ($P<0.01$ *vs.* MPC and sham treatment; $P<0.001$ *vs.* hydrogel implantation), while there was no difference with fibers, and, notably, with nonoperated controls (Fig, 5*B*, bottom panel). It should be noted that myosin BF-G6, an isoform of embryonic myosin used as a marker of regenerative processes (22), was still present in various clusters of GFP^+ myofibers 6 wk after treatment with both fibers and SCs delivered in HA-PI, showing that neofiber maturation was still ongoing (Fig. 5*C*).

While the regeneration of contractile fibers is of pivotal importance in muscle tissue engineering, functional integration remains dependent on the formation

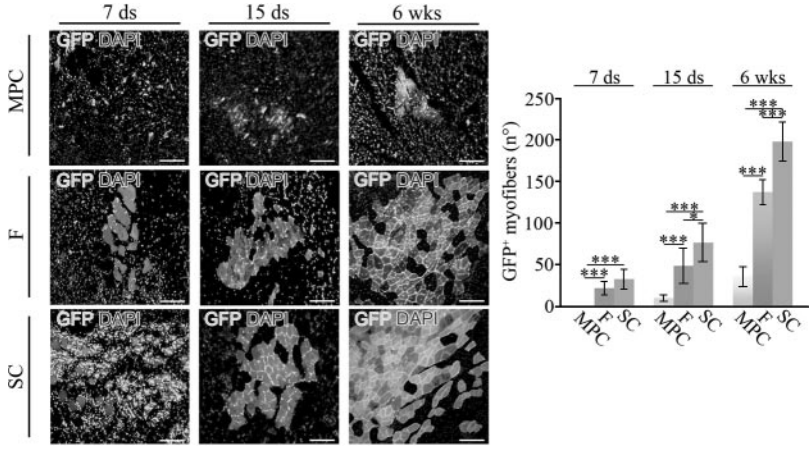

Figure 4. Contribution to regeneration of donor myogenic precursors. Left panel: epifluorescence for GFP (plus DAPI) on muscles treated with 1.5×10^5 cultured MPCs, 20 single fibers (F), or 250 freshly isolated SCs at 7 d, 15 d, and 6 wk postoperation. Scale bars = 100 μm. Right panel: quantification of GFP^+ myofibers confirmed a better engraftment when SCs were used. $*P < 0.05$; $***P < 0.001$.

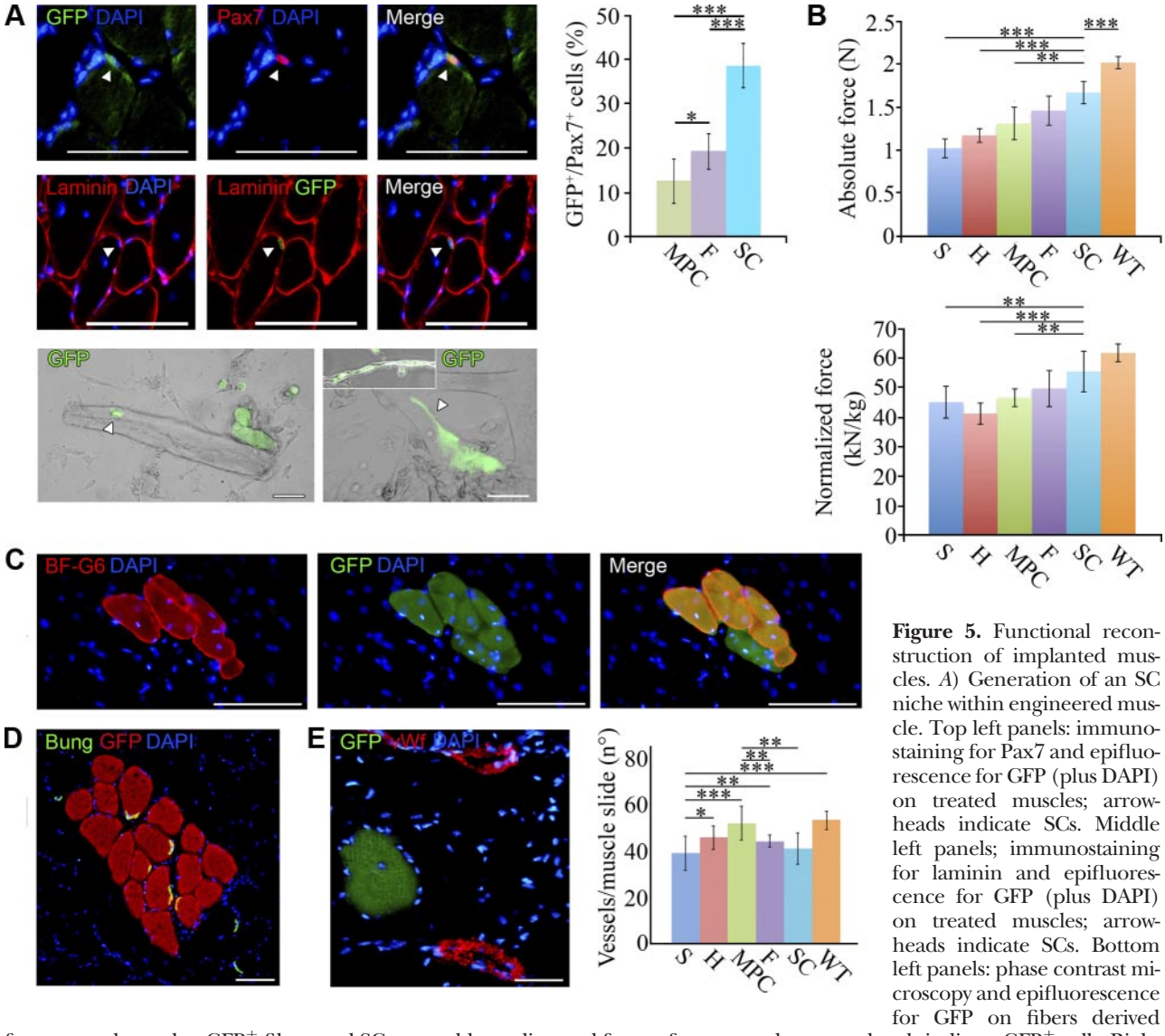

Figure 5. Functional reconstruction of implanted muscles. *A*) Generation of an SC niche within engineered muscle. Top left panels: immunostaining for Pax7 and epifluorescence for GFP (plus DAPI) on treated muscles; arrowheads indicate SCs. Middle left panels; immunostaining for laminin and epifluorescence for GFP (plus DAPI) on treated muscles; arrowheads indicate SCs. Bottom left panels: phase contrast microscopy and epifluorescence for GFP on fibers derived from treated muscles. GFP^+ fibers and SCs were able to align and fuse to form myotubes; arrowheads indicate GFP^+ cells. Right panel: $GFP^+/Pax7^+$ cells in muscles treated with 1.5×10^5 cultured MPCs, 20 single fibers (F), and 250 freshly isolated SCs further demonstrated better muscle reconstitution when SCs were used. *B*) Force measurement on treated muscles compared to untreated controls. Measurements were carried out 6 wk after treatment. Top panel: absolute force values (N) in the different conditions. S, sham; H, HA-PI alone, MPC, HA-PI with 150,000 cultured MPCs; F, HA-PI with 20 single fibers; SC, HA-PI with 250 freshly isolated SCs; WT, wild-type untreated animals. Bottom panel: normalized force-weight values (kN/kg) in the different conditions. *C*) Left panel: immunostaining for embryonic myosin isoform BF-G6. Center panel: epifluorescence for GFP. Right panel: merge of left and center images. *D*) Immunostaining for 488-bungarotoxin identifying neuromuscular junctions, and anti-GFP (plus DAPI). *E*) Left panel: immunostaining for von Willebrand factor and epifluorescence for GFP (plus DAPI) to mark blood vessels. Right panel: quantification of the number of vessels per muscle slide in the different treatment conditions. Scale bars = 100 μm. $^*P < 0.05$; $^{**}P < 0.01$; $^{***}P < 0.001$.

of both neuronal and vascular networks. This has represented a major limitation in previous studies (2, 23), and growth factors have been suggested to improve nerve regeneration (24) and new capillary formation (25, 26). In our experimental model, treated muscles showed the presence of neuromuscular junctions on both GFP^+ and GFP^- myofibers, as demonstrated through labeling with fluorescent α-bungarotoxin (Fig. 5*D*). Vascularization of the engineered tissue was monitored by immunostaining for von Willebrand factor; the number of vessels obtained was somewhat lower than that found in controls (Fig. 5*E*).

DISCUSSION

Reconstruction of organs, and, specifically, of skeletal muscle, is a difficult task (2, 3). Here, we show how, combining freshly isolated SCs (8, 9) and an innovative, photopolymerizable hydrogel (20), we were able to promote histological and functional reconstruction of a partially ablated skeletal muscle.

The initial part of our work focused on the characterization of the properties of our novel type of hydrogel. In particular, our physicochemical analyses demonstrated that this formulation would be well suited both

for delivery *via* open access (as was the case of our experimental design) and *via* needle injection. The former case would be applicable in tissue engineering approaches aimed at repairing gross muscle damage, such as cases of orthopedic or oncologic surgery. Delivery *via* direct injection could instead be of use in all those instances in which it would be desirable to implant myogenic cells without damaging the recipient muscle, *e.g.*, cell-based therapies for muscular dystrophies. In this latter case, photopolymerization could easily be achieved by using optic fibers channeled into the needles.

The *in vivo* degradation rate of the cell-carrying scaffold is a crucial parameter in muscle engineering; on one hand, the matrix must protect the newly injected myogenic cells from the potentially harmful effect of the host's innate immune response cells in the initial hours after transplant (27), but on the other hand, it should disappear gradually as the newly formed myofibers reclaim the muscle's volume. In our experimental protocol, the initial volume of the hydrogel implant was ~3–4 times larger than that of the removed muscle (due to technical constraints, we could not resuspend our cells in <15 μl of solution). Still, hydrogel was almost completely gone in 8 d; such finding confirmed that, as desired, hydrogel was present in the muscle only during the massive first wave of inflammation after damage (from 2 to 4 d; see ref. 28) and was, therefore, suitable for protecting delivered myogenic cells before fiber formation. Another very important feature of hydrogel was its very chemical composition. In fact, hyaluronic acid is not simply a biocompatible material, but it is already known to exert positive effects in the context of tissue repair, and hyaluronic acid-based materials are already used in surgical procedures. In our case, the reduction of fibrosis that we detected 6 wk after surgery in the hydrogel-treated muscles *vs.* the sham-operated controls was in agreement with such properties (Fig. 3*B*).

At present, it is generally accepted that SCs have much better engrafting and regenerative potential compared to *in vitro* expanded myogenic precursor cells when it comes to muscle cell transplantation (9). Still, to the best of our knowledge, this is the first report of a direct comparison of the two cell types in the context of tissue engineering. Here, we demonstrated that muscle reconstruction could be achieved much more efficiently when using freshly isolated SCs instead of MPCs and that by transplanting just ~250 SCs, we could restore normal muscle architecture plus reconstitution of the muscle stem cell niche throughout the whole muscle volume. It should be noted that in our experimental model, we were not able to perform a direct comparison with the delivery of cells alone (*i.e.*, without hydrogel) due to the nature of our surgical procedure. In fact, injecting a suspension of cells into the pocket created in the TAs would invariably lead to significant leaking in the suturing phase and, hence, to unpredictable variability in the regeneration outcome. On the other hand, the cells alone *vs.* cells in hydrogel comparison will pose no problem in the context of direct intramuscular injection, an experimental model that we are currently developing for dystrophic mice.

Muscle reconstruction in terms of newly generated myofibers is an essential target, but the engraftment of SCs in the host niche is even more important, due to its role in supporting subsequent cycles of regeneration, in particular, in the presence of congenital pathologies like muscular dystrophies (29). Here, we demonstrated that implanted SCs not only contributed to the formation of myonuclei but also repopulated the host niche. Besides, the finding that a large number of donor-derived SCs could be found associated with GFP^- fibers (see Supplemental Fig. S3) indicated that they had migrated away from the area of initial delivery and had reached fibers that had not incorporated donor-derived myonuclei, thereby suggesting an improved migration of delivered cells when compared to our previous results (11, 30). In this regard, we also noticed that SCs derived from injected MPCs were almost exclusively found associated with GFP^+ fibers, suggesting a lesser migration potential (Supplemental Fig. S3).

Notably, in our animals, the reconstructive process was associated with functional recovery, as muscles that had received stripped SCs showed no significant difference in contractile performance when compared to untreated controls. In agreement with this finding, regenerated areas showed the formation of proper nervous connections and vascularization. These results were quite satisfactory, especially when considering that regeneration was not yet complete in muscle treated with fibers and SCs (as indicated by the expression of embryonic myosine). At the same time, however, we realize that when dealing with the reconstruction of much larger masses of tissue (as it will be the case for applications in humans), vascularization and reinnervation in the engineered muscle will likely need to be improved. This could be achieved in our system by spiking the HA-PI with microspheres containing growth factors (31) or by genetically engineering implanted cells (2).

In summary, we have shown for the first time that hydrogel technology, which was previously successfully used for functional recovery of ischemic heart tissue (32), can also be applied in skeletal muscle. On the basis of the results obtained, we conclude that using HA-PI to deliver SCs is a promising approach for the reconstruction of diseased or damaged muscles. FJ

The authors gratefully acknowledge Fidia Advanced Biopolymers (Abano Terme, Padua, Italy) for providing HA-PI. This work has been supported by Fondazione Telethon (Rome, Italy; grant GGP07216), Fondazione Il Sangue (Milan, Italy) and Fondazione Città della Speranza (Malo, Vicenza, Italy; grant 08/02). P.D.C. has been supported by the Great Ormond Street Hospital Charity. C.A.R., M.F., M.P., C.R., L.V., N.E. and P.D.C. designed the experiments; C.A.R., M.F., B.B., E.F., and L.V. performed the experiments; C.A.R., L.V., N.E., and P.D.C. wrote the article. The authors declare no competing financial interests.

REFERENCES

1. Rosenblatt, J. D., Lunt, A. I., Parry, A. J., and Partridge, T. A. (1995) Culturing satellite cells from living single muscle fiber explants. *In Vitro Cell. Dev. Biol. Anim.* **31,** 773–779
2. Yan, W., George, S., Fotadar, U., Tyhovych, N., Kamer, A., Yost, M. J., Price, R. L., Haggart, C. R., Holmes, J. W., and Terracio, L. (2007) Tissue engineering of skeletal muscle. *Tissue Eng.* **13,** 2781–2790
3. Rossi, C. A., Pozzobon, M., and De Coppi, P. (2010) Advances in musculoskeletal tissue engineering: moving towards therapy. *Organogenesis* **6,** 767–772
4. Mauro, A. (1961) Satellite cell of skeletal muscle fibers. *J. Biophys. Biochem. Cytol.* **9,** 493–495
5. Seale, P., and Rudnicki, M. A. (2001) A new look at the origin, function, and "stem-cell" status of muscle satellite cells. *Dev. Biol.* **218,** 115–124
6. Dhawan, J., and Rando, T. A. (2005) Stem cells in postnatal myogenesis: molecular mechanisms of satellite cell quiescence, activation and replenishment. *Trends Cell Biol.* **15,** 666–673
7. Beauchamp, J. R., Morgan, J. E., Pagel, C. N., and Partridge, T. A. (2000) Dynamics of myoblast transplantation reveal a discrete minority of precursors with stem cell-like properties as the myogenic source. *J. Cell Biol.* **22,** 1113–1122
8. Montarras, D., Morgan, J., Collins, C., Relaix, F., Zaffran, S., Cumano, A., Partridge, T., and Buckingham, M. (2005) Direct isolation of satellite cells for skeletal muscle regeneration. *Science* **309,** 2064–2067
9. Collins, C. A., Olsen, I., Zammit, P. S., Heslop, L., Petrie, A., Partridge, T. A., and Morgan, J. E. (2005) Stem cell function, self-renewal, and behavioral heterogeneity of cells from the adult muscle satellite cell niche. *Cell* **29,** 289–301
10. Cima, L. G., Vacanti, J. P., Vacanti, C., Ingber, D., Mooney, D., and Langer, R. (1991) Tissue engineering by cell transplantation using degradable polymer substrates. *J. Biochem. Eng.* **113,** 143–151
11. Boldrin, L., Elvassore, N., Malerba, A., Flaibani, M., Cimetta, E., Piccoli, M., Baroni, M. D., Gazzola, M. V., Messina, C., Gamba, P., Vitiello, L., and De Coppi, P. (2007) Satellite cells delivered by micro-patterned scaffolds: a new strategy for cell transplantation in muscle diseases. *Tissue Eng.* **13,** 253–262
12. Serena, E., Flaibani, M., Carnio, S., Boldrin, L., Vitiello, L., De Coppi, P., and Elvassore, N. (2008) Electrophysiologic stimulation improves myogenic potential of muscle precursor cells grown in a 3D collagen scaffold. *Neurol. Res.* **30,** 207–214
13. Beier, J. P., Stern-Straeter, J., Foerster, V. T., Kneser, U., Stark, G. B., and Bach, A. D. (2006) Tissue engineering of injectable muscle: three-dimensional myoblast-fibrin injection in the syngeneic rat animal model. *Plast. Reconstr. Surg.* **118,** 1113–1121
14. Hathcock, J. J., Hall, C. L., and Turitto, V. T. (2000) Active tissue factor shed from human smooth muscle adheres to artificial surfaces. *J. Biomater. Sci. Polym. Ed.* **11,** 1211–1225
15. Cleland, R. L., and Wang, J. L. (1970) Ionic polysaccharides. 3. Dilute solution properties of hyaluronic acid fractions. *Biopolymers* **9,** 799–810
16. Huang, L. K., Mehta, R. C., and DeLuca, P. P. (1997) Evaluation of a statistical model for the formation of poly [acryloil hydroxyethyl starch] microspheres. *Pharm. Res.* **14,** 475–482
17. Rossi, C. A., Pozzobon, M., Ditadi, A., Archacka, K., Gastaldello, A., Sanna, M., Franzin, C., Malerba, A., Milan, G., Cananzi, M., Schiaffino, S., Campanella, M., Vettor, R., and De Coppi, P. (2010) Clonal characterization of rat muscle satellite cells: proliferation, metabolism and differentiation define an intrinsic heterogeneity. *PLoS One* **5,** e8523
18. Blaauw, B., Mammucari, C., Toniolo, L., Agatea, L., Abraham, R., Sandri, M., Reggiani, C., and Schiaffino, S. (2008) Akt activation prevents the force drop induced by eccentric contractions in dystrophin-deficient skeletal muscle. *Hum. Mol. Genet.* **17,** 3686–3696
19. Salic, A., and Mitchison, T. J. (2008) A chemical method for fast and sensitive detection of DNA synthesis in vivo. *Proc. Natl. Acad. Sci. U. S. A.* **105,** 2415–2420
20. Revell, P. A., Damien, E., Di Silvio, L., Gurav, N., Longinotti, C., and Ambrosio, L. (2005) Tissue engineered intervertebral disc repair in the pig using injectable polymers. *J. Mater. Sci. Mater. Med.* **18,** 303–308
21. Freed, L. E., Vunjak-Novakovic, G., Biron, R. J., Eagles, D. B., Lesnoy, D. C., Barlow, S. K., and Langer, R. (1994) Biodegradable polymer scaffolds for tissue engineering. *Biotechnology (N. Y.)* **12,** 689–693
22. Schiaffino, S., Gorza, L., Sartore, S., Saggin, L., and Carli, M. (1986) Embryonic myosin heavy chain as a differentiation marker of developing human skeletal muscle and rhabdomyosarcoma. A monoclonal antibody study. *Exp. Cell. Res.* **163,** 211–220
23. De Coppi, P., Bellini, S., Conconi, M. T., Sabatti, M., Simonato, E., Gamba, P. G., Nussdorfer, G. G., Parnigotto, P. P. (2006) Myoblast-acellular skeletal muscle matrix constructs guarantee a long-term repair of experimental full-thickness abdominal wall defects. *Tissue Eng.* **12,** 1929–1936
24. Rumsey, J. W., Das, M., Kang, J. F., Wagner, R., Molnar, P., and Hickman, J. J. (2008) Tissue engineering intrafusal fibers: dose- and time-dependent differentiation of nuclear bag fibers in a defined in vitro system using neuregulin 1-beta-1. *Biomaterials* **29,** 994–1004
25. De Coppi, P., Delo, D., Farrugia, L., Udompanyanan, K., Yoo, J. J., Nomi, M., Atala, A., and Soker, S. (2005) Angiogenic gene-modified muscle cells for enhancement of tissue formation. *Tissue Eng.* **11,** 1034–1044
26. Borselli, C., Storrie, H., Benesch-Lee, F., Shvartsman, D., Cezar, C., Lichtman, J. W., Vandenburgh, H. H., and Mooney, D. J. (2009) Functional muscle regeneration with combined delivery of angiogenesis and myogenesis factors. *Proc. Natl. Acad. Sci. U. S. A.* **107,** 3287–3292
27. Qu, Z., Balkir, L., van Deutekom, J. C., Robbins, P. D., Pruchnic, R., Huard, J. (1998) Development of approaches to improve cell survival in myoblast transfer therapy. *J. Cell Biol.* **142,** 1257–1267
28. Malm, C. (2001) Exercise-induced muscle damage and inflammation: fact or fiction? *Acta Physiol. Scand.* **171,** 233–239
29. Blau, H. M. (2008) Cell therapy for muscular dystrophy. *N. Engl. J. Med.* **359,** 1403–1405
30. Carnio, S., Serena, E., Rossi, C. A., De Coppi, P., Elvassore, N., Vitiello, L. (2011) Three-dimensional scaffold allows long-term wild-type cell delivery in dystrophic muscle. *J. Tissue Eng. Regen. Med.* **5,** 1–10
31. De Jong, S.J., van Eerdenbrugh, B., van Nostrum, C.F., Kettenes-van den Bosch, J.J., Hennink, W.E. (2001) Physically crosslinked dextran hydrogels by stereocomplex formation of lactic acid oligomers: degradation and protein release behavior. *J. Control. Release* **71,** 261–275
32. Giraud., M.N., Ayuni, E., Cook, S., Siepe, M., Carrel, T. P., Tevaerai, H. T. (2008) Hydrogel-based engineered skeletal muscle grafts normalize heart funtion early after myocardial infarction. *Artif. Organs* **32,** 692–700

Received for publication October 19, 2010.
Accepted for publication March 10, 2011.